JOURNAL OF PROPULSION AND POWER
Vol. 14, No. 4, July–August 1998

Beamlet Profiles from Multiple-Hole Ion-Extraction Systems

Yukio Hayakawa,* Shoji Kitamura,* and Katsuhiro Miyazaki†
National Aerospace Laboratory, Tokyo 182-8522, Japan

Ion-beamlet structures were studied experimentally to find the conditions for which ion beamlets had noncircular profiles. Seven or less ion beamlets were extracted from a discharge chamber using a multiple-circular-hole ion-extraction system that was composed of a pair of screen and accelerator grids. A beam separator was employed to eliminate all but one ion beamlet. The isolated ion beamlet was observed three dimensionally using arrayed Faraday probes, which showed that the ion-beamlet profiles were distorted hex-symmetrically under certain conditions. To measure the degree of distortion a distortion factor was introduced. The ion beamlet was generally a superposition of a circular-profiled beamlet consisting of the major part of the ions and a distorted-profiled beamlet consisting of the minor part of the ions. Attempts to demonstrate the hex-symmetrical profile computationally using a conventional three-dimensional numerical ion-extraction model that assumed a constant ion density over all of the ion-trajectory origins failed, but the results indicate that inclusion of nonuniform ion production would solve the problem.

Nomenclature

d_a = accelerator-hole diameter, mm
d_s = screen-hole diameter, mm
d_{sp} = beamlet-separator-hole diameter, mm
F_d = distortion factor, s/S
J_b = beamlet current, A
l_{cc} = hole-center-to-center distance, mm
l_e = effective acceleration length, mm
l_g = screen-to-accelerator-grid separation, mm
l_{sp} = accelerator-grid-to-separator separation, mm
NP/H = normalized perveance per hole
R = net-to-total voltage ratio (V_n/V_t), $A/V^{3/2}$
S = beamlet-profile area (standard-circle area), mm^2
s = area outside of standard-circle beamlet profile, mm^2
t_a = accelerator-grid thickness, mm
t_g = screen-grid thickness, mm
V_a = accelerator-grid voltage, V
V_d = discharge voltage, V
V_n = net accelerating voltage ($\cong V_d + V_s$), V
V_s = screen-grid voltage, V
V_t = total accelerating voltage ($V_n - V_a$), V

Introduction

THE shapes of worn ion-thruster accelerator-grid holes[1,2] suggest that a hexagonally symmetric distortion of ion-beamlet current density profiles occurs. Because the distortions of each beamlet profile are in phase azimuthally, the composite profile of the complete ion beam is also distorted.[3,4] This indicates that typical cross-sectional ion-beam diagnostics are not capturing the character of the full beam and that three-dimensional ion-beam diagnostics are required to correctly estimate beam-divergence angle. However, three-dimensional diagnostics are extremely complex, and it is sometimes impossible to set a three-dimensional-diagnostics apparatus in an existing facility. By comprehending the distortion of the ion beamlet, the beam-divergence angle may be estimated using cross-sectional diagnostics or the distortion itself can be avoided. An attempt to simulate this phenomenon numerically,[5] which was initiated before the present study began, yielded results that can be used to illustrate important effects. Typical results in Figs. 1 and 2 show trajectory data for a single ion beamlet. Figure 1 shows ion trajectories that start upstream of the screen grid and end on various boundaries. The top and bottom lines in Fig. 1 represent boundaries between regions of analysis for adjacent beamlets, and boundaries on the upstream and downstream ends define the region of analysis. Figure 2 shows intersections between selected ion trajectories and virtual planes at the upstream faces of the screen and accelerator grids. The hexagonal borders on these figures represent boundaries between adjacent beamlets. The trajectories that hit the screen grid are represented by the dots outside of the screen hole. The dots within the accel hole in Fig. 2 represent ion trajectories that cross the virtual plane on the upstream face of the accelerator-grid face. For the particular case illustrated none of the trajectories hit the accelerator grid.

Assumptions associated with the numerical ion-extraction model[5] were 1) the ion velocity at the upstream boundary was equal to the ion mean thermal velocity and was perpendicular to the screen-grid face, and 2) the ion density was constant over the upstream boundary. Each ion trajectory represents the same number of ions and they were distributed uniformly on the upstream boundary. The hexagonal distribution of the dots on the upstream screen-grid face suggests that this distribution is hexagonal in the plane of the virtual face at the upstream side of the screen grid. The trajectories beyond the edge of the screen-grid hole are, however, intercepted and the resulting circular-beamlet pattern remains relatively circular through the accelerator hole. Figure 2 reveals, however, that there are noncircular features and an azimuthal nonuniformity in the accel-hole, ion-beamlet pattern. This is because, at least in part, of the polygonal elements employed in the numerical model, but this computational inaccuracy does not appear to be sufficient to explain the observed nonuniformity. Consequently, another explanation for the distortion was sought. It has been shown experimentally that hexagonal screen holes cause distorted beamlet profiles.[6–8] This same phenomenon was demonstrated using the computer program. It was also observed that actual holes in ion-engine screen grids become slightly hexagonal during manufacturing because the grid webbing yields where it is thinnest during the pressing step that follows hole etching. This effect is most significant for the outermost holes in the grid. Computational studies showed that even slight distortions of a screen hole resulted in a badly distorted ion-beamlet pat-

Received June 3, 1996; presented as Paper 96-3199 at the AIAA/ASME/SAE/ASEE 32nd Joint Propulsion Conference, Lake Buena Vista, FL, July 1–3, 1996; revision received Jan. 21, 1998; accepted for publication Jan. 21, 1998. Copyright © 1998 by the American Institute of Aeronautics and Astronautics, Inc. All rights reserved.

*Senior Research Officer, Space Technology Research Group. Member AIAA.
†Senior Research Officer, Space Technology Research Group.

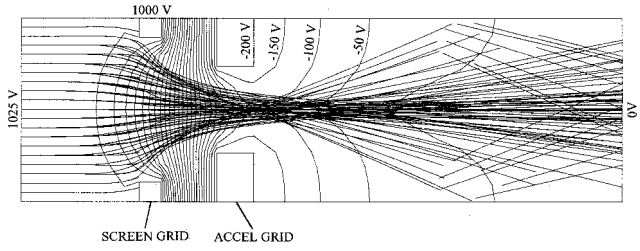

Fig. 1 Ion trajectories and equipotential contours (computer generated).

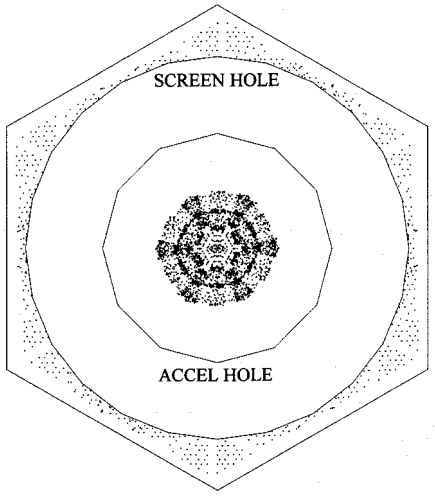

Fig. 2 Beamlet profile at screen- and accelerator-grid face (computer generated).

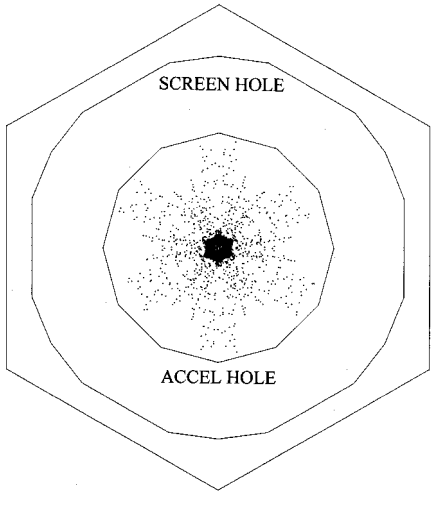

Fig. 3 Beamlet profile from semihexagonal screen hole (middle started, computer generated).

tern. An example of this is shown in Fig. 3, where the distribution of ions are observed to exhibit substantial hexagonal distortion.

The preceding numerical investigation seemed adequate to show that the pattern of the screen-grid holes itself was causing the distorted ion-beamlet pattern. It was argued that even screen holes modeled as perfectly circular would yield the observed distortions and that the computer model could be applied to predict not only macroscopic parameters like divergence angles and deflection angles, but also to understand the microscopic mechanisms of ion extraction. The objective of this research was originally to verify this postulate, and a preliminary experiment was conducted at the beginning of the study to show that circular screen holes could produce distorted ion-beamlet profiles. Subsequently, the objective became one of finding conditions that yielded noncircular ion-beamlet patterns and developing a model that simulated the details of the ion-extraction process. This paper describes the experimental apparatus, procedures, and results used to establish the source of the observed beamlet distortion. The implications of the results for numerical simulations of ion-thruster beams are discussed and techniques for avoiding distortion identified. Finally a summary of the major conclusions is provided.

Apparatus and Procedure

Ion Source

A cutaway drawing of the ion source used in this study is shown in Fig. 4. It consists of a discharge chamber from a 14-cm xenon ion thruster equipped with screen and accelerator grids that each have a centerline hole surrounded by six others. All of the screen-grid holes were electric-discharge machined so that the distortion of mechanical drilling would be avoided. The conical-beamlet separator, which is shown downstream of the accelerator grid, had a 30-deg half-angle and it intercepted all beamlets except the one at the thruster centerline. Direct ion impingement on this separator was insignificant. The separator was held at ground potential so that it played a role similar to that of a decelerator grid in a three-grid system. Figure 5 defines symbols that represent the dimensions of the ion-extraction system. The distance between the accelerator grid and separator, which is not indicated, was not precisely controlled. The photograph of the separator after the experiments (Fig. 6) reveals six dimples etched by the off-centerline beamlets, but there is no sign of significant ion impingement from the centerline beamlet near the cone apex. This suggests

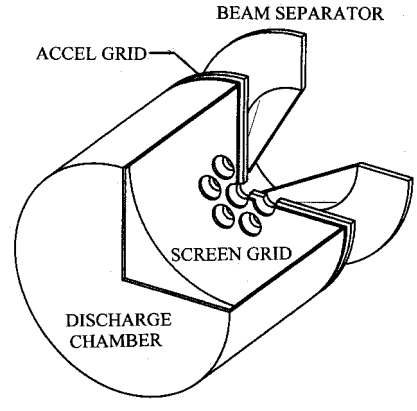

Fig. 4 Ion source and beam separator.

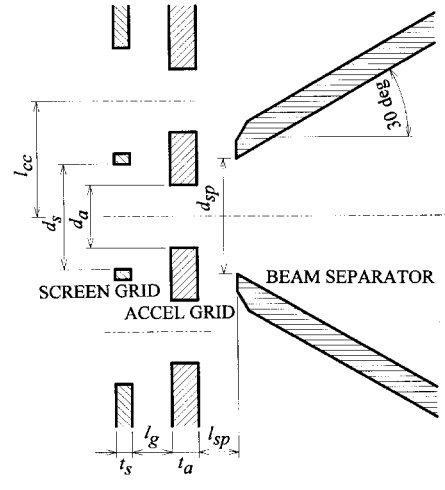

Fig. 5 Ion extraction system dimensions.

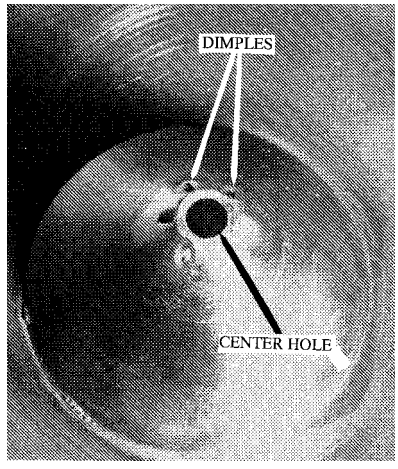

Fig. 6 Beam separator after experiment.

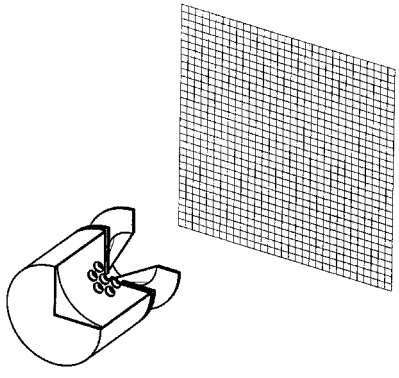

Fig. 7 Intersections showing probe positions.

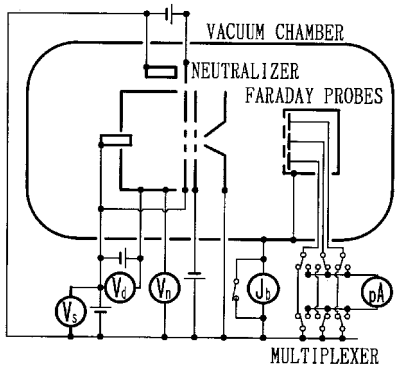

Fig. 8 Electric schematic of ion thruster and diagnostics.

that the separator did not affect the shape of the center-hole ion beamlet.

Arrayed Faraday Probes

Thirty-two, 8-mm-diam-orificed Faraday probes, arrayed vertically at 1-cm intervals on an $X-Y$ stage were used to measure ion-beamlet current-density profiles. The probes were moved perpendicularly to the beamlet axis in 1-cm increments to obtain ion-current densities at the intersections of the 32 by 32 (1024 point) array shown in Fig. 7. Measurements were repeated at several axial locations. Two ammeters (Keithley 486 and 487) connected to a computer were used to measure and record the probe currents. The ammeters were operated in parallel and each was equipped with a mechanically relayed multiplexer that switched it through the 16 probes. Collection of a complete data set required about 2 min. Probe currents were sensed by single measurements made through in-line analog and digital filters.

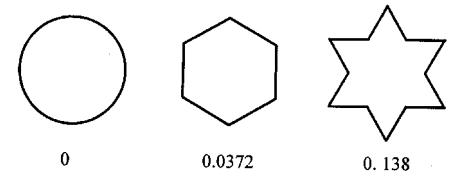

Fig. 9 Shapes and corresponding distortion factors.

Electrical Equipment

An electrical schematic of the ion source and test facility is shown in Fig. 8. An ammeter is shown that measures the ion-beamlet current J_b, and its reading depended strongly on the neutralizer condition, and so it could not be used reliably. This occurred because some electrons emitted from the neutralizer reached the vacuum-chamber wall and affected the measurement. The ion-beamlet current was obtained summing the 1024 probe currents. This current was independent of the neutralizer condition because a grounded plate was placed in front of the neutralizer, so that emitted electrons would not go directly to the Faraday probes.

Definitions

There are three ways to define normalized perveance per hole.[9–11] In this study, it is defined as

$$\frac{NP}{H} = \frac{J_b}{V_t^{3/2}} \left(\frac{l_e}{d_s} \right)^2$$

where l_e is defined as

$$l_e = \left(l_g^2 + \frac{d_s^2}{4} \right)^{1/2}$$

Distortions in the azimuthal uniformity of the ion beamlet are expressed using the concept of a distortion factor, which is determined using the following procedure:

1) Determine the area of the targeted beamlet profile pattern (S).

2) Draw a circle that is centered on the pattern at the maximum-ion-current-density location and has the same area as the pattern. This circle is called the standard circle.

3) Determine the area of pattern that falls outside the standard circle and inside the outline of the pattern (s).

4) Compute the distortion factor using $F_d \equiv s/S$.

Distortion factors corresponding to three outlines are shown in Fig. 9. It is noteworthy that distortion factors never reached zero because data analysis was accomplished numerically and circles were represented as polygons.

Divergence angles are represented as half-angles of cones that enclose 95% of the beamlet current and are determined using the following procedure:

1) Select the largest probe current among 1024 probe currents using a partial-averaging method and designate the position of this probe as the beamlet center.

2) Arrange the 1024 probe currents in order of angle from the beamlet center to the radial location of the probe measured from the beamlet center.

3) Add up the probe currents sequentially until the sum reaches 95% of the beamlet current, thereby determining the angles on either side of the one that corresponds to 95% of the beamlet current.

4) Determine the divergence angle by interpolating between these angles.

Error Estimation

The accuracy of probe-current measurements is affected by the accuracy of the ammeters and by noise that may originate

Table 1 Hole-center-to-center distances and grid separation

l_{cc} mm (l_{cc}/d_s)	l_g mm (l_g/d_s)
4.4 (1.1)	1.5 (0.375) standard case
4.4 (1.1)	2.0 (0.5)
4.4 (1.1)	2.5 (0.625)
4.8 (1.2)	1.5 (0.375)
5.2 (1.3)	1.5 (0.375)
5.6 (1.4)	1.5 (0.375)

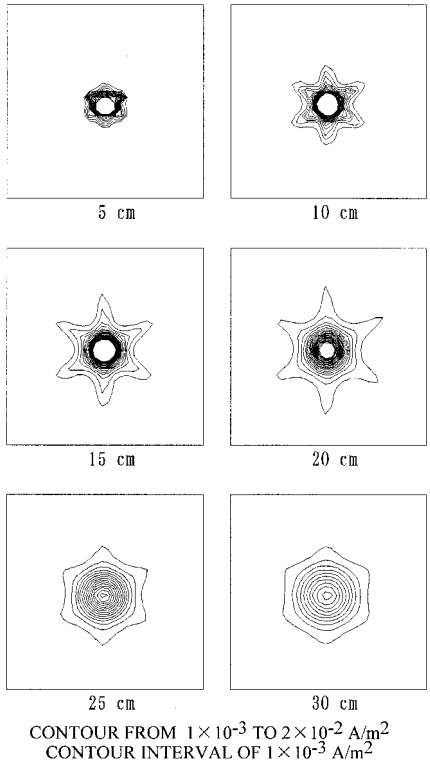

Fig. 10 Ion-current-density contours (standard case).

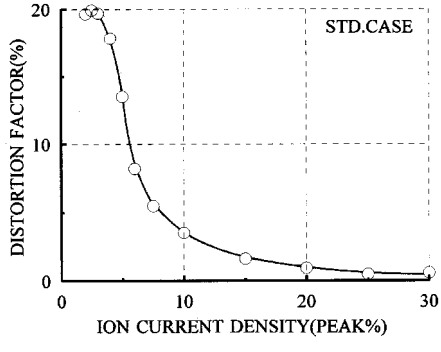

Fig. 11 Distortion factors at various contour levels.

as electrical noise and fluctuations in beamlet and background-plasma conditions. In each test, the meter scale was set to give at least a four-digit resolution and this resulted in random current fluctuations no greater than the one-hundredth (generally less than one-thousandth) of the largest current. The inaccuracy of the ammeters was insignificant compared to that caused by noise. Changing the value of the largest probe current by 1% (0.025% change in the current density) has an insignificant effect on the distortion factor. Even though the contours were not smooth in low perveance cases, the distortion factors were generally reproducible and beam current determined by summing the probe currents were reproducible to within 1%. Probe currents, particularly those associated with the peaks, were sensitive to probe position, as discussed next.

The spatial resolution of the measurement restricts both the resolutions of the distortion factor and divergence angle. Both resolutions generally decrease as the divergence angle decreases if the spatial resolution is fixed. In this study, the resolution error in the divergence angle is theoretically less than 0.35 deg when the divergence angle is larger than 10 deg. In practice, the peak-position variation must also be considered, and the errors because of it are estimated to be less than 1.5%

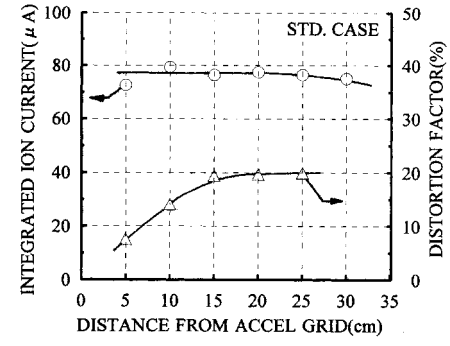

Fig. 12 Integrated ion-beamlet current and distortion factor.

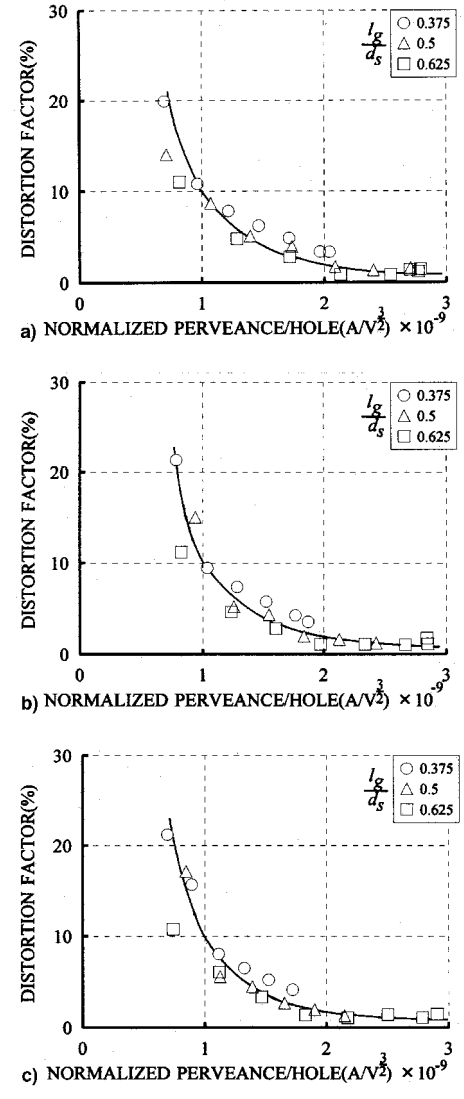

Fig. 13 Effects of grid separation and accelerator-grid voltage on distortion factor: a) $V_a = -200$ V ($R = 0.837$), b) $V_a = -300$ V ($R = 0.774$), and c) $V_a = -400$ V ($R = 0.719$).

for the distortion factor and less than 0.5 deg for the divergence angle. The error introduced by representing a smooth curve as segments in calculating the distortion factor is included in the preceding value.

The total errors are estimated to be less than 1.5% for the distortion factor and less than 0.85 deg for the divergence angle over all perveance values.

Experimental Results

The following are the operating parameters and grid dimensions held constant: propellant gas = xenon, background pressure = 4.0–5.1 $\times$ 10^{-4} Pa (N_2); V_a = −200 (standard case), −300, −400 V; V_s = 1000 V; V_d = 17–23 V; d_a = 2.4 mm; d_s = 4.0 mm; d_{sp} = 4.4 mm; l_{sp} = ~1 mm; t_a = 1.0 mm; and t_s = 0.6 mm. Table 1 shows grid dimensions (hole-center-to-center distances and screen-to-accelerator-grid separations) that were varied in this study. The normalized perveance per hole was always calculated using a net-accelerating voltage of 1025 V on the basis that the discharge plasma potential should be a few volts greater than the anode-to-ground voltage difference. Figure 10 shows ion-current-density contours measured for the standard case (V_a = −200 V, l_{cc} = 4.4 mm, and l_g = 1.5 mm) on planes located at 5-cm intervals over the range 5–30 cm downstream of the accel grid. The variation in distortion factors defined using ion-current-density contours a distance of 25 cm from the accelerator grid is shown in Fig. 11. The value that represents each contour can be chosen arbitrarily between zero and the peak current density, and the horizontal axis of Fig. 11 shows the percentage of the value to the peak current density. The beamlet profile was distorted only where the ion-current density was low, whereas it was almost circular where the density was high. This shows that the distorted-profiled beamlet was a superposition of a circular-profiled beamlet consisting of the major part of ions and a distorted-profiled beamlet consisting of the minor part of ions. The distortion factor of the ion beamlet is determined from the 2.5%-ion-current-density contour after this. The integrated ion-beamlet current and distortion factor associated with Fig. 10 are shown in Fig. 12. The closer the measuring plane was to the ion source, the lower the number of effective measuring points. This made the integrated current and distortion factors unreliable when close to the grid. In contrast, in the case of the measuring plane being too far from the ion source, the ion beamlet might bulge out of s, causing excessively low integrated currents and deficient contours. In this research, the 25-cm far plane is used to determine the integrated currents and distortion factors.

Figure 13 shows the effects of the grid separation and accelerator-grid voltage on the distortion factor. The distortion is observed to decrease as perveance is increased and, because all of the data points fall along a common curve, it can be

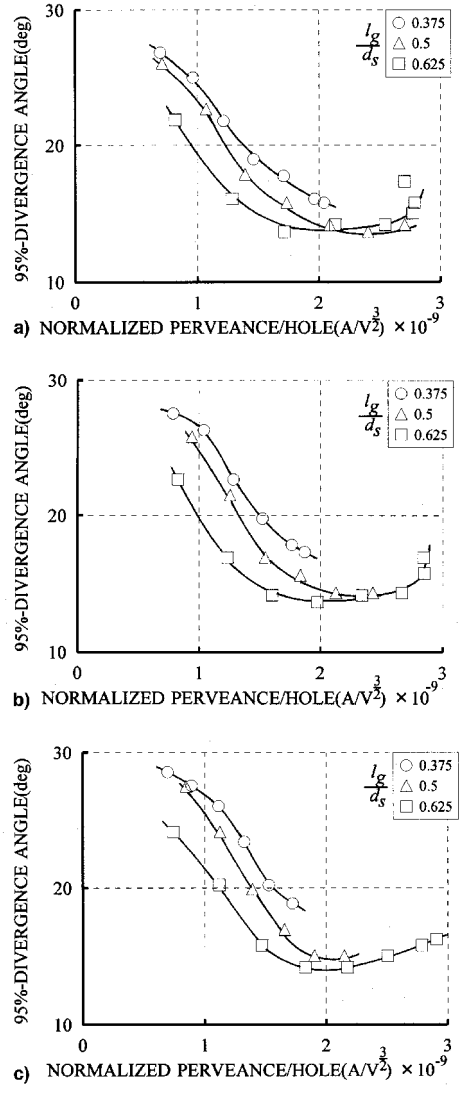

Fig. 14 Effects of grid separation and accelerator-grid voltage on divergence angle: a) V_a = −200 V (R = 0.837), b) V_a = −300 V (R = 0.774), and c) V_a = −400 V (R = 0.719).

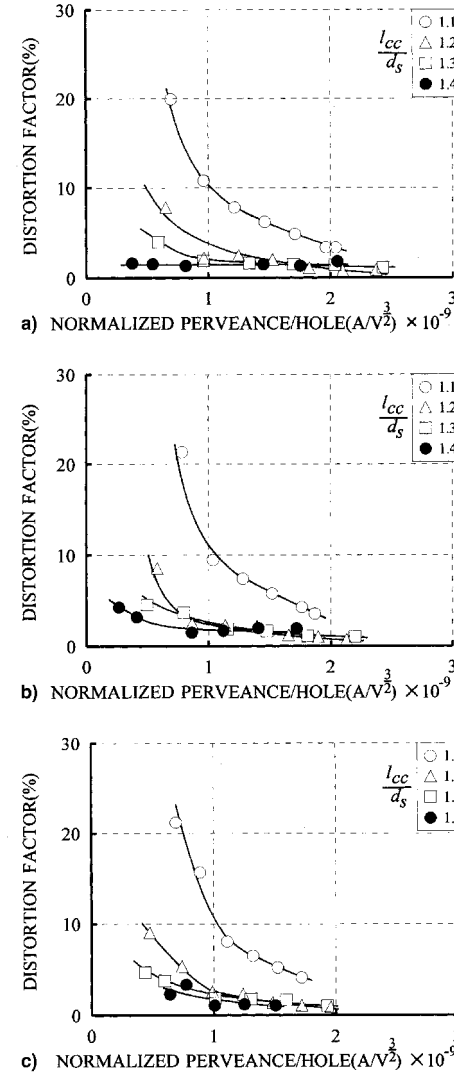

Fig. 15 Effects of hole-center-to-center distance on distortion factor: a) V_a = −200 V (R = 0.837), b) V_a = −300 V (R = 0.774), and c) V_a = −400 V (R = 0.719).

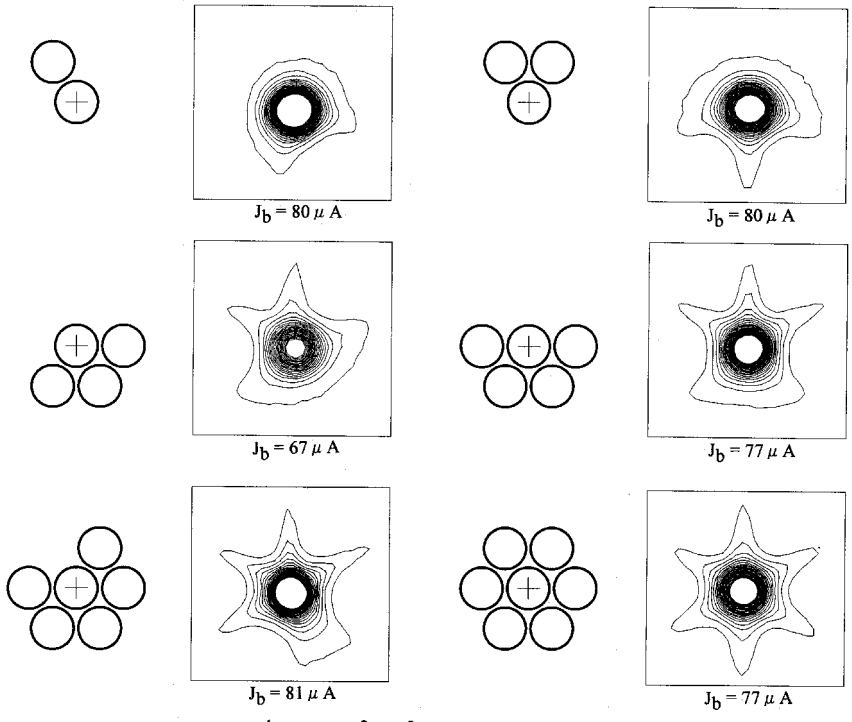

Fig. 16 Contour deformation because of neighboring hole(s) (standard case).

concluded that distortion factor is independent of both the accelerator-grid voltage and grid separation. It is noted, however, that this independence is related to the definition of normalized-perveance-per-hole and other definitions would not necessarily exhibit this independence.

The data of Fig. 14 show the general trend for divergence angle to decrease with perveance to a minimum value and then rise slightly as perveance is increased. They also show consistent trends in divergence angle as grid separation and accelerator voltage are changed.

Figure 15 shows the effects of the hole-center-to-center distance on the distortion factor. In general they show that distortion decreases as perveance is increased, but this is caused, in part, by the fact that signal-to-noise ratios are low at low perveances. Data obtained at the greatest hole-separation ratio (l_∞/d_s = 1.4) are noteworthy because they show that the distortion remains both low and relatively constant as perveance is varied. This indicates that the beamlet profile is not distorted hex-symmetrically when the holes are far apart.

Figure 16 shows corresponding arrangements of screen holes and ion-current-density contours observed as the number of screen holes adjacent to a central one was changed from 1–6. The contours shown were selected because they corresponded to integrated ion currents J_b that were close to that for the standard case (77 μA). As the correspondence between hole arrangements and patterns suggests, the hole induces asymmetry on the side of the beamlet opposite the holes. This indicates that it is the ion trajectories that cross over the beamlet axis that have their trajectories altered by adjacent holes. The concave contours were not just deficient circles, but they extended beyond the expected circles at both sides of the deficits.

Discussion

Reliability of Numerical Analyses

Because ion behavior during extraction cannot be observed directly, numerical analyses are required and the accuracy of models associated with these analyses can be verified only by comparing predictions with measurable quantities such as divergence and deflection angles with measured values. Such comparisons showed that computed and experimental divergence angles agreed well,[5] but the model failed to show distorted beamlet contours like those shown in Fig. 10. Possible reasons why the distortions were not computed include the following:

1) Some input constants, e.g., initial ion velocity, ion density, etc., were invalid.

2) The model was too simple, e.g., the number of ion trajectories modeled was too small, the finite elements were too coarse, etc.

3) The model was physically incorrect.

To compare computed and experimental results, the computed and measured beamlet currents must agree. Beamlet current is controlled through the initial ion velocity, and the ion i.e., plasma, density and analysis showed that essentially identical results were obtained over reasonable ranges of initial velocity and density, provided their product was held constant. Recall that ions were all assumed to start with a velocity corresponding to the mean thermal velocity and perpendicular to and significantly upstream of the screen grid. This model may seem to be oversimplified, but it is considered adequate because ion thermal velocities are at most an order-of-magnitude less than 0.1 eV, and this is negligible because they pass through volt-level potential differences between the upstream plasma and the screen grid. Consequently, introducing random velocities will complicate the computations without affecting the results significantly.

It was found that the distances between the upstream boundary of the region being analyzed and the upstream screen-grid face as well as that between the downstream accelerator-grid face and the downstream boundary affected analytical results. They did not, however, affect the azimuthal distortion of the beamlet patterns. It was also found that the number of the ion trajectories used in the analysis had a minor effect on this distortion. It should be noted that grid holes are modeled as polygons rather than circles because finite element modeling was used. This introduced some distortion (Fig. 2), but did not seem to have a significant effect on the gross shapes of the beamlet patterns. This hole-shape distortion seemed greatest at low perveances, but even there the azimuthal phase associated

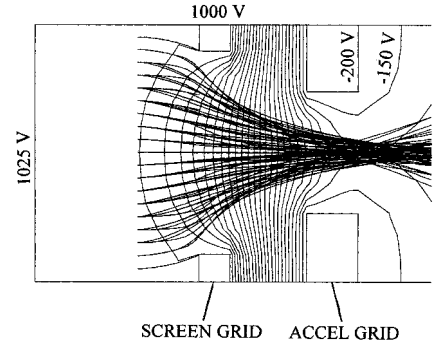

Fig. 17 Trajectories of middle-started ions and equipotential contours (computer generated).

with it was different from those acquired experimentally by 30 deg and it tended to cancel the natural distortion associated with the hexagonal adjacent-hole distortion.

Origin of Beamlet Ions that Yield a Distorted Pattern

It has been suggested that the numerical model was improper. The fact that a distorted-profiled beamlet consisted of a major circular-profiled part of ions and a minor distorted-profiled part of ions suggests that the model was not essentially but partially improper. The numerical model lacked the ions that composed the distorted-profile part, and it would work only by introducing an adequate number of ions into the right position in the upstream region. In the numerical model, no ions were assumed being produced in the region of analysis, in other words, near the screen grid. An attempt to find the origin of these ions was made by introducing the ions into this region in various ways.

First, the ions were put uniformly on a plane between the upstream boundary and the screen grid that was parallel to the screen-grid face with a very small velocity heading downstream. This means that these ions were uniformly produced near the screen grid. An electric field was assumed as already being determined from the ions started at the upstream boundary, and the charges of the ions started in the middle were not assumed to affect the electric field for the simplicity of the computer program. The last assumption was partially justified from the fact that the distorted-profiled-part ions were minor. This attempt was only for seeking a possibility and no information to determine the density of the middle-started ions was obtained. Typical middle-started-ion trajectories are shown in Fig. 17. The result associated with Fig. 17 was essentially the same as that with Fig. 2, and no expected distortion was obtained. For semihexagonal screen holes, the ions starting in the middle had a larger impact on beamlet profile distortion than the ions started at the upstream boundary. These results showed that the uniformly produced ions had little influence on the beamlet distortion. The preceding result indicates that ions produced nonuniformly close to the screen hole caused the distorted part of the beamlet. Strictly speaking, ions appear to be produced locally in the region near the upstream face of the screen-grid-webbing triangles. It is known that some of the electrons have high enough energy to reach the screen grid.[12] It is likely that these electrons ionize neutral atoms while heading for the webbing triangles where potential barriers are lower than elsewhere. This mechanism can explain the extensions of contours in Fig. 16. Where there was no neighboring hole, the high-energy electrons heading downstream could uniformly reach the screen grid while they were forced to concentrate at the triangles where there were neighboring holes. Analyzing the beamlet-ion energy may test the existence of this mechanism. The ion energy in the rim region of the distorted profile is expected to be some volts lower than that in the center region.

The discharge plasma has been experimentally investigated at the neighborhood of the screen grid, but no information about the differences between the region over the webbing triangle and elsewhere was presented.[13] The density distribution of the ions produced over the triangle is not known, and so constructing a numerical ion-extraction model that includes these ions is difficult. A numerical ion-production model is required before constructing the numerical ion-extraction model.

Avoiding the Distortion

The beamlet distortion is undesirable for ion thrusters because it may increase beam divergence and damage the accelerator grids. This research shows it can be quite easily avoided by raising the normalized perveance per hole or hole-center-to-center distance (in practice, keeping the distance constant and decreasing the hole diameters). In fact, some ion thrusters produce almost circular-beam profiles.[14,15]

Conclusions

Ion-extraction systems composed of only circular holes sometimes produce hex-symmetrical-profiled ion beamlets. Ion beamlets can be modeled as a superposition of a circular-profile ion beamlet including the major part of ions and a distorted-profiled ion beamlet including a small fraction of the ions. Experimental results obtained using a seven-hole ion-extraction system showed that both the distortion factor and divergence angle increased as the normalized perveance per hole was decreased when the perveance was low, but only the divergence angle increased and the distortion factor remained small as the perveance was increased when the perveance was high. The distortion of the beamlet could be avoided by increasing the perveance or hole-center-to-center distance. Numerical results showing that uniform ion production cannot generate the observed profile indicate that ions that formed the distorted-profiled beamlets were expected to originate from over the screen-grid-webbing triangles.

References

[1]Brophy, J. R., Pless, L. C., and Garner, C. E., "Ion Engine Endurance Testing at High Background Pressures," AIAA Paper 92-3205, July 1992.

[2]Hayakawa, Y., Miyazaki, K., and Kitamura, S., "Performance Test of a 14-cm Xenon Ion Thruster," AIAA Paper 92-3147, July 1992.

[3]Nakanishi, S., "Diagnostic Evaluations of a Beam-Shielded 8-cm Mercury Ion Thruster," NASA TM-78855, April 1978.

[4]Groh, K. H., Fahrenbach, P., and Loeb, H. W., "Tests on the European Primary Radio-Frequency Engine ESA XX," AIAA Paper 94-3391, June 1994.

[5]Hayakawa, Y., "Three-Dimensional Numerical Model of Ion Optics System," *Journal of Propulsion and Power*, Vol. 8, No. 1, 1992, pp. 110–117.

[6]Byers, D. C., and Banks, B. A., "Beam Focusing Characteristics of Variously Shaped Grid Holes," NASA TM X-67922, Sept. 1971.

[7]Fearn, D. G., Stewart, D., Harbour, P. J., Williams, J., and Davis, G. L., "The UK 10 cm Mercury Ion Thruster Development Program," AIAA Paper 75-389, March 1975.

[8]Rawlin, V. K., "Characterization of Ion Accelerating Systems on NASA LeRC's Ion Thrusters," AIAA Paper 92-3827, July 1992.

[9]Kaufman, H. R., "Technology of Electron Bombardment Ion Thrusters," *Advances in Electronics and Physics*, Vol. 36, Academic, New York, 1974, pp. 265–373.

[10]Kaufman, H. R., "Accelerator-System Solutions for Broad-Beam Ion Sources," *AIAA Journal*, Vol. 15, No. 7, 1977, pp. 1025–1034.

[11]Homa, J. M., "Ion Beamlet Steering for Two-Grid Electrostatic Thrusters," NASA CR-174671, July 1984.

[12]Hayakawa, Y., Miyazaki, K., and Kitamura, S., "Measurements of Electron Energy Distributions in an Ion Thruster," *Journal of Propulsion and Power*, Vol. 8, No. 1, 1992, pp. 118–126.

[13]Aston, G., and Wilbur, P. J., "Ion Extraction from a Plasma," *Journal of Applied Physics*, Vol. 52, No. 4, 1981, pp. 2614–2626.

[14]Myers, R. M., Pencil, E. J., Rawlin, V. K., Kussmaul, M., and Oden, K., "NSTAR Ion Thruster Plume Impacts Assessments," AIAA Paper 95-2825, July 1995.

[15]Tierney, C. M., Brophy, J. R., and Mueller, J., "Segmented Ion Engine Plume Characteristics," AIAA Paper 94-2740, June 1994.